Local durability optimization of a large-scale direct methanol fuel cell: catalyst layer tuning for homogeneous operation and in-operando detection of localized hydrogen evolution

C. Rabissi*[a], M. Zago[a], L. Grahl-Madsen[b], M. Odgaard[b], A. Casalegno[a]

[a] Politecnico di Milano, Department of Energy, Via Lambruschini 4, 20156 Milano, Italy

[b] IRD Fuel Cells A/S, Emil Neckelmanns Vej 15 A&B, 5220 Odense, Denmark

*corresponding author: claudio.rabissi@polimi.it

Abstract

Lifetime limitations are still penalizing direct methanol fuel cell technology, otherwise outstandingly promising for sustainable portable power generation. Strong heterogeneous performance fading related to uneven operating conditions is known to be exacerbated in the upscaling processes towards commercial applications, especially at local level. This work applies a localized optimization strategy, previously developed on lab scale samples, on a commercial 180 cm^2 membrane electrode assembly, analysing both current and potential distribution by means of a custom macro-segmented fuel cell provided with array of reference electrode. Analysis based on local polarization curves and impedance spectroscopy demonstrates that water distribution, leading to local dehydration as well flooded areas, drives uneven operation and fading. Consequently, platinum loading at cathode electrode has been redistributed, sensibly improving current density heterogeneity and stability (from 148 to 53.8 $\mu V\ h^{-1}$) over a 600 h degradation tests. Then, residual fading identified at outlet regions has been investigated by means of local potential analysis, demonstrating a highly uneven operation of both electrodes. This phenomenon is discussed as the evidence of localized hydrogen evolution, which is identified for the first time during nominal galvanostatic operation and suspected to contribute to uneven fading of components.

Keywords:

Degradation, direct methanol fuel cell, heterogeneity, hydrogen evolution, local optimization

1. Introduction

Direct methanol fuel cell (DMFC) is a promising technology for stationary and portable energy applications from very small to medium scale (e.g., portable electronics to off-grid applications), as well as for light and industrial vehicular sectors. The high energy density of liquid methanol, which also enables a convenient, safe and quick recharging [1–3], constitutes unmatched advantage for such applications. However, the spread of such technology is hindered by several drawbacks, among which the severe degradation of cathode catalyst layer (CCL) and the non-negligible rate of methanol crossover through the membrane that limit both durability and efficiency of the technology [4,5].

Beneath the mentioned issues, cathode degradation is regulated by a complex interplay of different physical phenomena which are strongly affected by locally varying operating conditions, which effect is a heterogeneous CCL degradation. Moreover, the issue can be exacerbated in the upscale process of the membrane-electrode assembly (MEA) from lab-scale to commercially meaningful sizes, which is known to be a non-trivial, complex development task, usually leading to considerably lower cell performance [6,7]. Hence, research effort on DMFC degradation is recently evolving towards locally-resolved analyses and larger scales MEAs or stacks [5,8–11]. Dixon et al. [10] used different analytical techniques to analyse the degradation of a DMFC stack membrane electrode assembly (MEA). A preferential precipitation of Ru was showed at the methanol outlet and the oxygen reduction reaction (ORR) activity was found to be reduced by the adsorption of Ru oxides on active Pt sites. Arlt et al. [11] applied a high energy resolution Synchrotron X-ray absorption edge imaging to study the aging of catalyst materials. Catalyst layer thickness was strongly influenced by the flow field geometry

and the structure of the gas diffusion layers (GDL): thinner catalyst layer was found under the ribs of the flow field and the crossing points of fiber bundles of the woven GDL. Hartmann et al. [9] analysed a 320 cm^2 MEA which has been used in a DMFC stack for more than 3000 h to power a lift truck. The local analysis of degradation with respect to the position on the flow field pattern was performed by cutting the MEA into 1 cm^2 pieces, that were subsequently characterized in a small test cell. Scanning electron microscopy analysis highlighted inhomogeneous thickness of aged catalyst layer and the degradation processes within the fuel cell were demonstrated to be influenced by the operating conditions.

Recently, Rabissi et al. [12] coupled post-mortem analysis with in-situ local current and impedance measurements performed in a 25 cm^2 segmented cell hardware. Cathode dehydration and flooding was demonstrated to locally worsen performance at cathode inlet and outlet regions and to induce uneven current distribution. Moreover, cathode outlet exhibited severe electrochemical surface area (ECSA) loss. Hence, in a subsequent work [13], the authors developed a gradient MEA, featuring higher catalyst loading at both cathode inlet and outlet and lower loading in the central region of the cell, aiming to obtain homogeneous current distribution and limit degradation rate. Current distribution was 55% more homogeneous and was actively redistributable during operation by means of cathode air stoichiometry, resulting in 70% decreased degradation rate compared to the uniform CCL loading MEA [12] during a 500 h degradation test, with a homogenous fading of performance. An 18% lower Pt nanoparticle growth at cathode outlet and limited ionomer degradation at cathode inlet were also identified by ex-situ analyses (transmission electron microscopy and X-ray photoelectron spectroscopy), indicating locally mitigated fading mechanisms. The promising results of such methodology (which has been recently filed in a PCT patent application [14] by the authors) revealed the detrimental effect that uneven limitations can play

on overall performance and durability, which could reasonably be more severe in commercial MEAs, characterized by higher active areas.

Regarding the second abovementioned issue, reactants distribution is a critical aspect and may lead to local reactants starvation. In fact, DMFC are fed at the anode side with a liquid mixture of methanol and water and methanol permeates through the membrane from anode to cathode. As explained in [15,16], methanol oxidation at the cathode generates protons and electrons, which are locally consumed by the ORR, lowering the useful oxygen concentration within the CCL. In the literature [16,17], it has been demonstrated that in the cell region with insufficient air supply, the cell consumes current to produce hydrogen at the anode. Kulikovsky et al. [16] confirmed the electrolytic regime in a DMFC with a single straight channel and segmented electrodes, showing that the length of the galvanic domain increases with the airflow rate. Ye et al. [18] observed gas bubbles in the anode flow field of a DMFC at OCV with low oxygen concentration and detected the presence of hydrogen. In [19], Ye et al. investigated transient OCV behaviour during oxygen startup and interruption and demonstrated that hydrogen evolution leads to OCV overshoot. Rabissi et al. [20,21] developed an external array of reference hydrogen electrodes (RHEs) and investigated anode dynamics, identifying parasitic hydrogen evolution during air feed interruption. However, all these works [13-18] analyse hydrogen evolution in specific operating conditions able to appositely trigger the mechanism or cell configurations that are sensibly different from the ones adopted during real operation.

It is worth to mention that, particularly when dealing with samples upscale, the flow pattern of reactant distributors is of utter importance in determining local performance distribution; indeed, numerous works are present in the literature focusing on the identification of optimal distributor geometries [22–28]. In this work, instead, we intend to demonstrate that an alternative, or additional, approach can pursue local performance homogenization and stability

improvement by optimizing local properties of the MEA given a specific a flow pattern for the distributors. Such result would suggest that, even after the actual optimization of reactants flow pattern, a local optimization of MEA properties could enable further improvements and has to be considered for a complementary, thorough, upscale optimization.

To the authors' knowledge, no work in the literature proposes a local investigation of performance and degradation of large scale DMFC MEA combining current density and potential distribution during operation. This work proposes a local characterization of performance and durability of a commercially-meaningful scale DMFC MEA of 180 cm^2 active area, applying a macro-segmented cell approach combined with local RHEs analysis. Starting from the understanding of local limitations to performance and durability, a proper optimization of the CCL component is proposed, manufactured and tested, discussing its beneficial impact. Subsequently, local electrodes potential is analysed during operation to distinguish anode from cathode contribution, with a particular focus on the identification of local reactant starvation, eventually driving to local parasitic hydrogen evolution during galvanic operation.

2. Experimental

2.1 MEA, macro-segmented cell and RHEs setup

Experimental activities described in this work are performed on 180 cm^2 commercial MEAs (active area is 13x14 cm) manufactured and provided by IRD Fuel Cells A/S. The membrane is Nafion® 115 (127 μm thick), anode and cathode are carbon supported catalyst layers with an average loading of 1.8 mg cm^{-2} (Pt-Ru alloy) and 1.2 mg cm^{-2} (Pt), respectively. CCL employs the highly-graphitized carbon support proposed in [12], demonstrated to operate stably in DMFC application, featuring high and discontinuous cathode operating potential. On both sides,

Sigracet® SGL35DC diffusion layers (overall thickness 325 μm, 20% PTFE content, coated with microporous layer) are adopted.

A novel implementation of the macro-segmented fuel cell, previously designed and applied to 25 cm^2 lab scale MEA investigation [12,13], has been appositely developed to meet the commercial MEA active area. The flow-field, whose geometry cannot be discussed in detail due to confidentiality agreement, is composed by 25-channels serpentine shaped in three main branches, with two preheating sections. The flow field is divided into five-segments: considering the results of [12,13], indicating cathode inlet and outlet regions as critical for MEA operating, these areas were divided in two segments each, in order to have a higher local resolution on involved phenomena.

Segmented current collectors, consisting of 1.5 mm thick goldened copper plates, together with two 30 mm thick aluminium endplates, complete the cell assembly. It is kept together by means of 16 bolts tightened using a calibrated torque wrench, each insulated from the respective current collector by means of 220 μm self-adhesive PTFE-glass fiber layers. Endplates housed three 1/4'' diameter x 5'' long electrical heating cartridges, controlled by PID logic, carefully placed to have the active heating section evenly distributed between the cell segments. Temperature was measured in the plates in three locations each, to verify its homogeneous distribution.

To enable deeper investigation of electrode operations and permit a distinction between anode and cathode contributions to cell performance, external hydrogen reference electrodes (RHE) were connected in three position at both anode and cathode (inlet, centre, outlet). Holes for connecting RHEs were carefully machined on the flow field rib, in order not to perturb mass flow in the channel while permitting direct contact of the salt bridge with the GDLs. As discussed in [15,21], the *in situ* reference electrode was based on a salt bridge made from fully water-saturated Nafion® tubing, which directly connects the external surface of the GDL with

an external electrolyte solution in which a Gaskatel HydroFlex® reversible hydrogen electrode (RHE) was immersed. At the appropriate locations within the GDL, a small amount (about 2 μL) of Nafion® polymer solution was dispersed in order to realize the necessary proton conductive path to the catalyst layer.

2.2 Experimental equipment

The power control system of the macro-segmented fuel cell (mSFC) was based on a high accuracy 5-modules electronic load (5x Chroma ATE 63630-80-80, current uncertainty 0.1% + 0.06 A; voltage uncertainty 0.3% + 0.018 V) with waveform generation capability for impedance analysis.

The anode solution was fed by a peristaltic pump with a resolution of 1 rpm and a speed uncertainty of 0.5%; anode mass flow rate was measured with an uncertainty of 1%. The methanol solutions were produced mixing ultra-deionized water (0.055 μS cm^{-1}) continuously produced by a multi-stage water deionizer (model Adrona Crystal EX Trace) and methanol (grade 99.9%w), by using a secondary peristaltic pump (resolution of 1 rpm, a speed uncertainty of 0.5%). Methanol mixture recirculation was required for the sake of investigation sustainability: methanol solution concentration value was measured and fed to a closed-loop control logic, by a Micro MCS sensor manufactured by ISSYS (micro-MCS, density uncertainty 0.5 mg_{CH3OH} cm^{-3}). Before the recirculation, anode exhaust was filtered by means of ion exchange resin (model Amberlite IRN-150) to avoid accumulation of contaminants. The solution was then fed to the main tank, where the solution was continuously mixed by a magnetic stirrer.

At cathode, the airflow rate was controlled and measured by a calibrated mass flowmeter with range properly increased to 6 Ndm^3 min^{-1} (uncertainty 0.02 Ndm^3 min^{-1}). The relative humidity (RH) of airflow was controlled by means of a high-volume heated bubbler with heated

tubing. On the cathode exhaust RH%, temperature and CO_2 concentration (as a proxy of oxidized methanol crossover from anode side) were measured prior to disposal.

All the instruments output, cell segments voltage and RHEs (through 10 nF capacitors to filter high-frequency signal noise) were measured by means of a NI-USB 6218 acquisition board, while thermocouples output was recorded by means of a NI USB-9213.

A schematization of the described setup is reported in Figure 1 - Schematic diagram of the experimental setup.Figure 1.

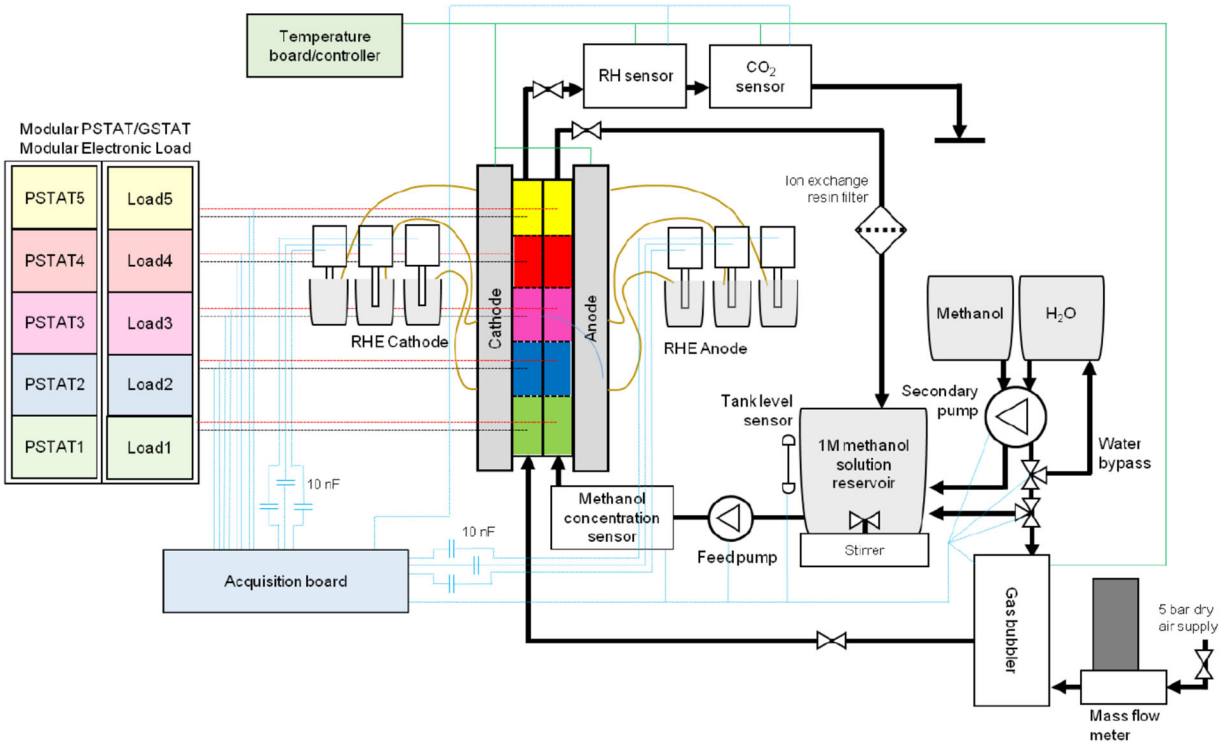

Figure 1 - Schematic diagram of the experimental setup.

2.3 Experimental tests

2.3.1 Polarization curve and EIS

DMFC local polarization curves were composed of 9 single measurement points from 0.01 to 0.4 A cm^{-2}, with each point being held for 600 s with reactants at constant flow rates (corresponding to λ_A=6 and λ_C=3 at 0.25 A cm^{-2}, unless where differently stated) to ensure steady state conditions. In agreement with manufacturer's recommendations, the adopted flow configuration was counter-flow.

After each period, a 60 s refresh cycle was performed to recover temporary degradation that may be accumulated during the measurement of the polarization curve itself, which could possibly affect measurement reliability. Cell voltage and potential of local RHEs were recorded and averaged as explained in [12] in order to obtain local iV curves and of the distribution of anode and cathode operating potentials. To verify consistency of the RHEs measurements, DMFC anode polarization curves were measured recording cell voltage with cathode fed with hydrogen, acting as a dynamic reference electrode (DHE) [12].

As discussed in [12,13], local electrochemical impedance spectroscopy (EIS) is measured at 0.1 and 0.25 A cm^{-2} during the iV curves, using the modular electronic load featuring current waveform generation and high-speed acquisition. The impedance is measured at 50 frequencies logarithmically spaced between 10 kHz and 50 mHz. In order to avoid any reciprocal interference between consecutive segments, accurate synchronous sinusoidal oscillation of the current density for all the segments is guaranteed. From the measurement of the four single local spectra, the overall cell impedance spectrum is calculated.

2.3.2 Degradation test

The m-SFC operated galvanostatically, as discussed in [12,13]: total current was divided by the 5-module electronic load between the segments, aiming to homogeneous voltage value (to limit parasitic crosscurrents between consecutive segments). Degradation testing was

performed at the nominal overall current density of 0.25 A cm^{-2} following a protocol to limit temporary degradation [12,13].

The operating protocol consisted of periods of 20 minutes galvanostatic operation interspersed by 1 minute of *refresh cycle*. The *refresh cycle* was composed by a sequence of an OCV and cathode air feeding interruption, intended to recovery temporary degradation during operation. During air feed interruption period, cathode potential was expected to drop below 0.5 V to reduce platinum previously oxidized [21].

Moreover, every 100 hours of operation a *full refresh* was performed to fully recover temporary degradation and perform iV curve measurement along with λ_C value optimization. The *full refresh* procedure, as described in [5], consisted of a ~16 h operation interruption under low mass flow of methanol solution (~0.3 g·min^{-1}) at anode electrode and was expected to restore liquid saturation of anode diffusion media. Cell temperature was maintained at 75°C with both cathode inlet and outlet manifolds plugged to avoid oxygen infiltration. As described in the following, λ_C was eventually adjusted during the break for diagnostics to keep homogeneous current density distribution: short operation periods of 5 minutes each were performed increasing λ_C up to 10% of the initial value, while measuring corresponding current density heterogeneity. The λ_C value leading to the most homogeneous distribution was adopted for the subsequent 100 h operation.

Degradation rate (expressed as a voltage decay rate in μV h^{-1}) is twofold evaluated from real-time operation and from iV curves, in compliance with JRC indications for test protocols [29]. During the end of each 100h operating period, voltage is recorded and linearly regressed, to calculate the voltage loss under load cycling. However, this value is affected by temporary degradation effects and is by the optimization of operating strategy (which modifies cathode stoichiometry λ_C, as already discussed). Hence, for a standardized and consistent evaluation of

permanent degradation rate, voltage loss is also calculated from i-V curves (performed after a *full refresh cycle*), which is always recorded at nominal operating conditions.

3. Results and discussion

In the following polarization curves and impedance spectra of the entire cell are represented with black dotted data points, while the local measurement of the five segments are indicated, moving from cathode inlet to outlet, in green, blue, purple, red and yellow solid curves, respectively.

Moreover, a heterogeneity level index of the current density *i* is defined as:

$$\varepsilon_i\ [\%] = \frac{\Delta i_{max}}{i} = \frac{i_{max} - i_{min}}{i}$$

where *i* is the average operating current density of the cell, while i_{max} and i_{min} are the values of current density provided by the highest and the lowest performing segment, respectively. The index ε_i is used in the following to quantify the dispersion of current density distribution among the segments.

3.1 Uniform MEA

The performance of the reference MEA with uniform platinum loading at cathode (UNF180-MEA) is analysed and discussed both in steady state and during 600h operation, highlighting local performance limitations and the respective impact on local stability of the component.

3.1.1 Steady state performance and EIS

Figure 2 shows local iV curves and the corresponding EIS of the UNF180-MEA. Interestingly, current density is distributed with strong analogies to the lab-scale sample previously investigated in [12]. Moreover, the same limiting mechanisms seem to regulate local cell operation with higher intensity.

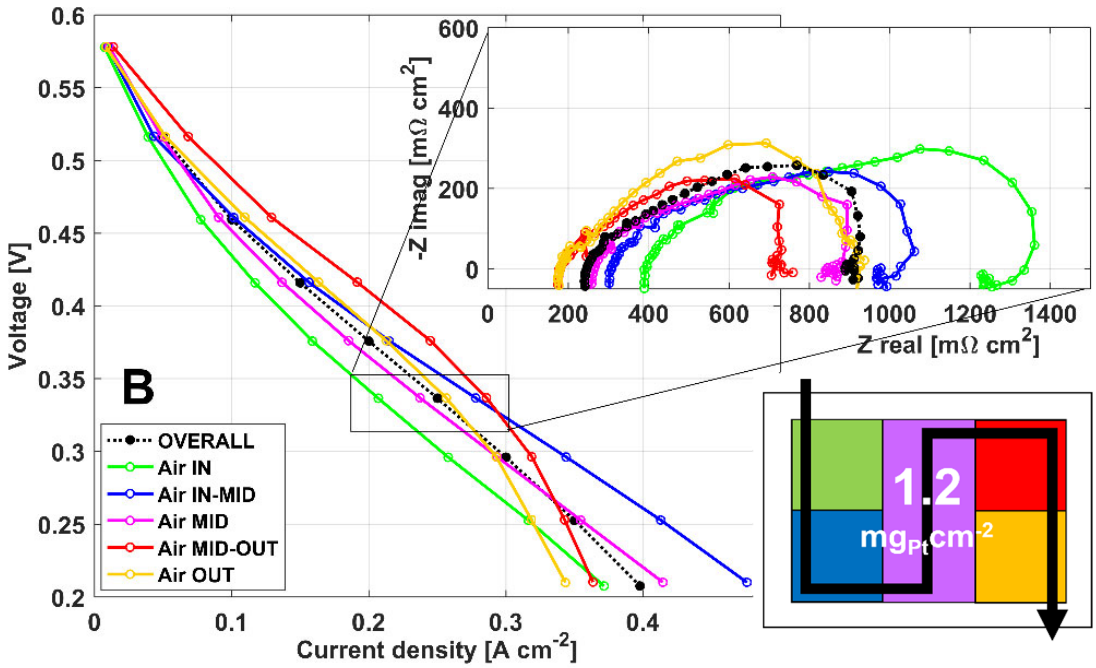

Figure 2 - Local and overall polarization curves, together with 0.25 A cm^{-2} local impedance spectra, for the UNF180-MEA component. The inset shows colour convention for the segments, together with local catalyst loading.

The counter-flow configuration, even though 35% more homogeneous than the co-flow configuration at nominal current density (reported as Figure S1 of supplementary material for the sake of shortness), still reveals a heterogeneous current density distribution ($\varepsilon_{0.25}$=31.6%). Air inlet area (depicted in green in Figure 2) appears to be strongly limited by dehydration: local high-frequency-resistance (HFR), equal to 396.1 mΩ cm^{-2}, is 50% higher than cell average HFR. Moreover, the corresponding EIS exhibits an elongation of the linear branch feature [30], leading the low-frequency real-axis intercept (LFR) of the local spectrum up to 1335 mΩ cm^{-2} (50% higher than cell average LFR). Air outlet area (depicted in yellow in Figure 2), highlights the onset of mass transport limitations around 0.2 A cm^{-2} leading to a sharp drop of performance at higher operating current. This behaviour is mainly caused by the lower oxygen availability at cathode outlet coupled with high water content (local HFR equal to 182.1 mΩ cm^{-2}).

This heterogeneous current density distribution has been confirmed to worsen at increased cathode stoichiometry (measured up to λ_C=6), because of the stronger limitations at cathode inlet region related to de-hydration.

The similarities between the results of the lab-scale 25 cm^2 MEA [12] with those of the commercial-scale 180 cm^2 MEA reveal the low influence of MEA dimension on the phenomena affecting current density distribution. Despite a seven times larger active area and a different flow-field geometry, water distribution still appears to play a crucial role in determining current density distribution, leading to the presence of de-hydrated as well as flooded regions, as it was concluded in [12].

The impact of such limitations on MEA durability is investigated in the following section, in order to aid the identification of the local optimization strategy to be applied.

3.1.2 Degradation analysis

Figure 3 shows cell voltage (A) and current density distribution (B) during a 600 h degradation test performed in reference counter-flow conditions at 0.25 A cm^{-2}, as discussed in section 2.3.2.

Cell voltage decay, as expectable from the strongly heterogeneous current density distribution (Figure 2), exhibits a fast-decreasing rate, interestingly following a linear trend. Operative voltage decay rate, evaluated as in the figure (A) from actual operation voltage as discussed in section 2.3.2, is equal to 147 μV h^{-1} and confirms the unoptimized cell operation. As a comparison, such value is much higher than the 56.4 μV h^{-1} degradation rate reported in the ground-breaking reference [31], relative to the degradation rate of 315 cm^2 MEAs as part of a 7 kW stack during the first 446 h operation period (successfully operated for 20.000 h in a forklift application). This evidences that the operation and stability of the UNF180-MEA, adopting the flow-filed configuration suggested by the manufacturer, need to be further investigated.

In agreement with the high dispersion measured in the polarization curve (Figure 2), the evolution of current density (Figure 3B) shows a very heterogeneous distribution, reaching its maximum value of $\varepsilon_{0.25,max}$=64% during the very first hours of operation. Strong redistribution of performance occurs during the 600 h degradation test, reaching a minimum of $\varepsilon_{0.25,min}$=44% at 220 h of operation. Major limitations arise from air outlet regions (red and yellow in Figure 3B), in which local current density decreases by roughly 40% in 600 h. Correspondingly, to ensure the overall galvanostatic operation, the local current density of air inlet and middle regions (blue, green and purple in Figure 3B) progressively increases. It is worth to mention that a more homogeneous redistribution of current density of the UNF180-MEA cannot be obtained by means of a regulation of cathode stoichiometry, since it would determine instead an increased dehydration of cathode inlet region, as demonstrated in [12] for the 25 cm^2 MEA and abovementioned for the UNF-180MEA in section 3.1.1 up to λ_C=6.

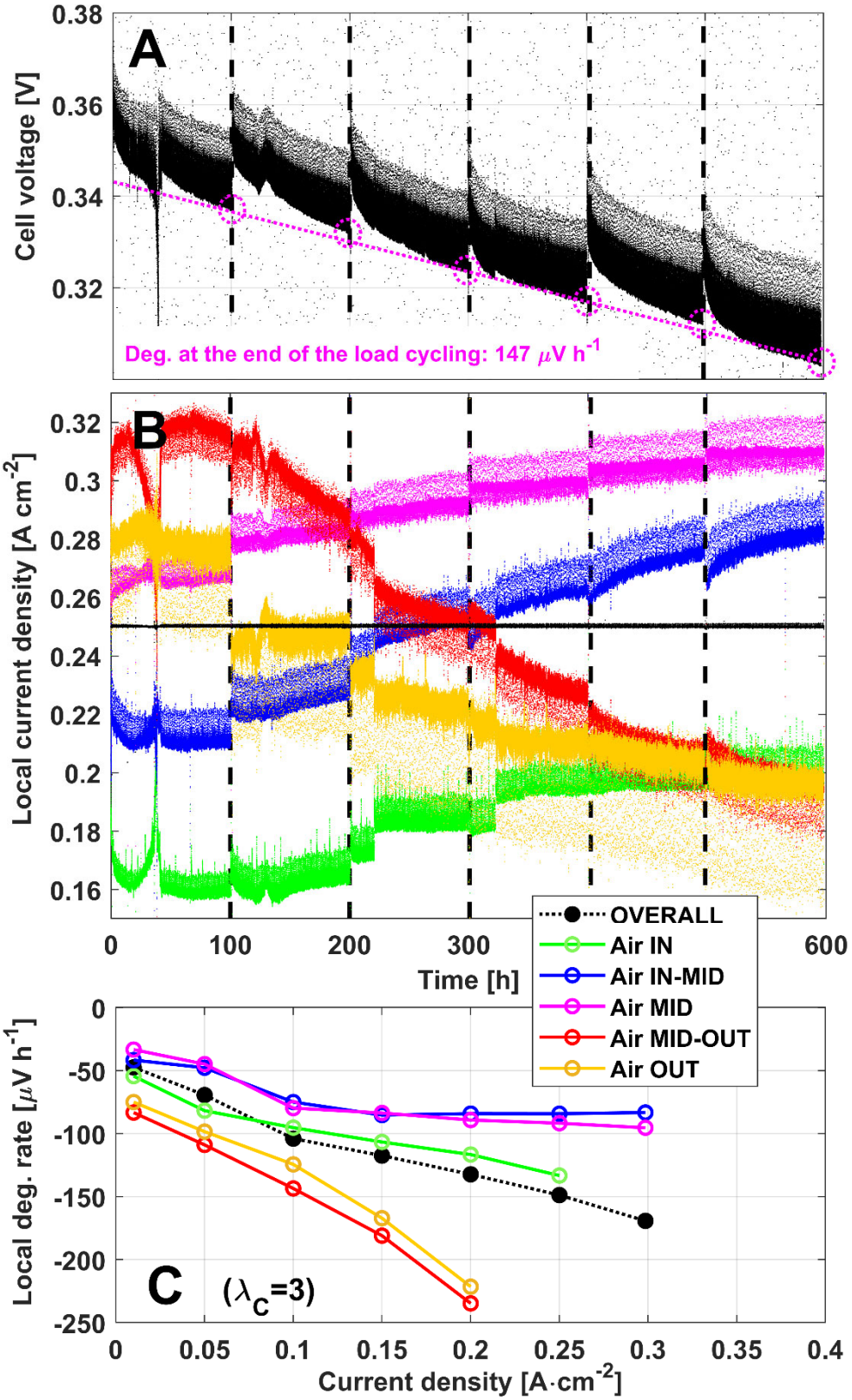

Figure 3 - Evolution during 600 h degradation test for the UNF180-MEA: A) cell voltage; B) local current density; C) overall and local permanent degradation rate at varying current density, calculated from BoL-EoT iV curves

From local CV analysis (reported as Figure S2A of the supplementary material for the sake of shortness), ECSA evolution shows a parabolic decreasing trend down to the 63% of the value at BoL (begin-of-life, 36.35 m^2g^{-1}). This decreasing trend is slightly more severe with respect to that of the 25 cm^2 lab-scale MEA investigated in [12], confirming a generally non-optimized operation for the UNF180-MEA.

Also, the evolution of local iV curves measured every 100 h during diagnostics interruption reveals a strong permanent degradation together with current density re-distribution. In order to highlight the local performance losses at each value of current density, voltage decay calculated from the difference between BoL (0 h) and EoT (end-of-test, 600 h) local iV curves is reported in Figure 3C as a degradation rate (148 $\mu V\ h^{-1}$ at 0.25 A cm^{-2}). A strong contribution to the overall performance degradation/loss appears to be due to cathode outlet regions, responsible for twice the overall loss evaluated at the maximum local current density.

3.2 Optimized MEA analysis

UNF180-MEA exhibited severe degradation during operation (Figure 3A) and the local performance analysis revealed a non-optimized operation due to the extreme operating conditions for both dehydration and flooding at cathode inlet and outlet, respectively (Figure 2). Thus, the optimization methodology presented in [13] for a 25 cm^2 lab-scale MEA and claimed in PCT patent application [14], is transferred to this larger MEA-scale on with a commercial flow path geometry.

3.2.1 Local optimization

In analogy to the cathode CL local optimization performed in [13], PRB180-MEA has been developed aiming to homogenize performance distribution at 0.25 A cm^{-2}. The inset of Figure 4 shows the PRB180-MEA, featuring a parabolic-like in-plane gradient for catalyst and ionomer

loading on cathode CL component. Loading has been increased at cathode inlet and outlet, correspondingly decreasing it at cell centre, while keeping the same average loading of the UNF180-MEA (1.2 mg cm^{-2}). Due to the extreme dehydration of cathode inlet and to the flooding of cathode outlet, local loading has been increased with different intensity in these regions of cell active area.

This leads to the loading distribution reported in Figure 4, with each segment loaded differently moving from inlet to outlet: 1.6, 1.2, 0.9, 1.2, 1.4 mg cm^{-2}, respectively. The so-called PRB180-MEA has been manufactured by IRD Fuel Cells A/S following the same process applied in [13], where the most proper technique to control the local loading of catalyst, carbon and ionomer was identified in the regulation of electrode local thickness. This strategy permits to maintain unchanged Pt/C and Ionomer/C ratios also without altering structure of the electrode such as the porosity.

The improved PRB180-MEA is subsequently tested analysing both local steady state performance and degradation.

3.2.2 Steady state performance and EIS

Figure 4 reports local iV curves together with local EIS spectra of the PRB180-MEA measured in reference operating conditions, directly comparable with those of UNF180-MEA (Figure 2).

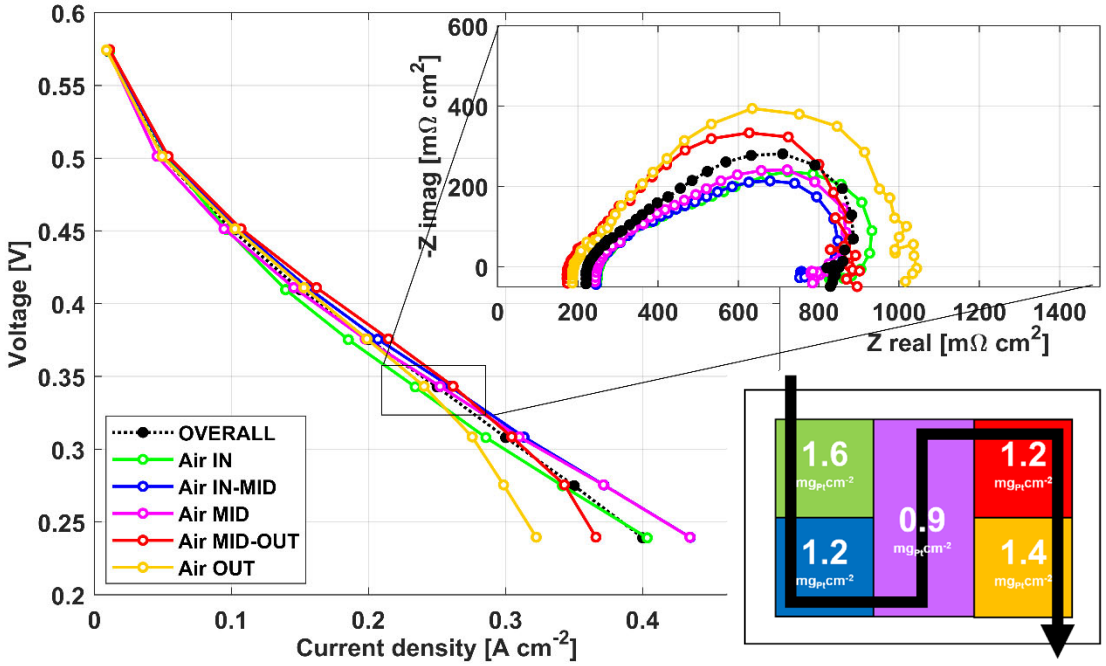

Figure 4 - Local and overall polarization curves, together with 0.25 A cm^{-2} local impedance spectra, for the PRB180-MEA component. The inset shows colour convention for the segments, together with local catalyst loading.

Clearly, the local optimization of catalyst and ionomer loading determines a sensible improvement of current density heterogeneity: the index of heterogeneity is reduced to $\varepsilon_{0.25}$=11%, considerably lower compared to the UNF180-MEA ($\varepsilon_{0.25}$=31.6%). Moreover, the PRB180-MEA shows a slight performance gain. Accordingly, local impedance spectra have a more even distribution in all the frequency range, as noticeable from the detail of Figure 4.

In particular:

- The most evident difference is related to the performance gain of cathode inlet area (depicted in green in Figure 4). The increase in catalyst and ionomer local loading appears to promote operation in dehydrated condition, enhancing water production and consequently self-hydrating the catalyst layer. Local current density at nominal cell current (0.25 A cm^{-2}) increases of about 21% from the UNF180-MEA to the PRB180-MEA samples.

Analysing EIS (green curve in the detail of Figure 4), local HFR value decreases to 255.6 mΩ cm^{-2}, close to cell average value, indicating an increased membrane hydration. At the same time, the high-frequency 45° linear branch feature [30,32] reduces its length at higher frequencies, indicating a local reduction of proton transport resistance in the catalyst layer. This leads to a $LFR_{PRB180\text{-}MEA}$ equal to 905 mΩ cm^{-2}, sensibly lower compared to the UNF180-MEA ($LFR_{UNF180\text{-}MEA}$=1335 mΩ cm^{-2}).

The same effects on both local iV curve and EIS are also noticeable on the air inlet-centre segment (depicted in blue in Figure 4), but with a lower magnitude, proofing that dehydration was formerly limiting performance almost up to cell central section.

- At air outlet, due to the increased oxygen consumption and water production at the inlet sections of the MEA, performance (yellow and red curves in Figure 4) is decreased from that of UNF180-MEA, getting local iV curves closer to those of cathode inlet region and hence contributing to homogenize current density distribution.

The ionomer and catalyst loading local increase at cathode inlet permits a more efficient operation even in presence of the strong dehydrating effect of the low-RH airflow. This, in strong analogy with the results obtained in [13], permits to use cathode stoichiometry as the optimization parameter for the control of current density redistribution. Indeed, differently from the behaviour of UNF180-MEA mentioned in section 3.1.1, increasing cathode stoichiometry above the reference conditions (measured up to λ_C=6) does not determine any performance loss localized at cathode inlet region, while instead determines a controllable performance gain at cathode outlet. Aiming to homogenize the performance distribution to its best, cathode stoichiometry has been experimentally optimized leading to the value of λ_C=3.15, corresponding to a heterogeneity index as low as $\varepsilon_{0.25}$=11%.

3.2.3 Degradation analysis

In order to demonstrate stability improvements obtained with the optimized local loading, a 600 h degradation test has been performed on the PRB180-MEA applying the optimized operating strategy. After having identified the operating condition leading to minimum heterogeneity in current density distribution, operating strategy has been correspondingly optimized. In analogy with [13], in order to contrast the tendency of current density distribution to shrink over cell active surface, cathode stoichiometry parameter has been adjusted during the degradation test for the PRB180-MEA. The actual need to adjust the stoichiometry has been experimentally verified during each operational break for diagnostics, periodically performed every 100 h.

The positive effect on current density distribution is verified analysing the response to a step-by-step variation of cathode stoichiometry; the operating value has been periodically adjusted to the one leading to the most homogeneous performance distribution at 0.25 A cm^{-2}.

Figure 5A reports the voltage decay trend during 600 h of degradation test on the PRB180-MEA performed following the optimized protocol (black dots), compared with the voltage loss of the analogous test performed on the UNF180-MEA (green dots). The comparison reveals a brilliant improvement of performance stability which, even though not reaching yet a satisfying level in absolute terms, decreases to roughly one third of that of the reference UNF180-MEA. Overall degradation rate regressed from operation voltage decay is 49.8 μV h^{-1}, against 147 μV h^{-1} measured for the UNF180-MEA. Hence, after local optimization, degradation rate is comparable to the one reported in [31] and already discussed (56.4 μV h^{-1} in the operating period 0-446 h), which is an important result also considering the lower catalyst loading and higher nominal current density adopted in the MEA utilized in the present work.

Figure 5B, depicts local current density evolution. The adjustment of operating conditions, performed in correspondence of the 400 h and 500 h interruptions and indicated by the purple

lines, consists in the increase of airflow respectively from λ_C=3.15 to λ_C=3.4 and then to λ_C=3.5. As noticeable, these adjustments help the redistribution of local performance: in particular, local current density related to the outlet areas of the MEA (depicted in yellow and red in Figure 5B) increases.

Comparing the current distribution dispersion with that of UNF180-MEA (Figure 3B), here not superimposed for sake of understandability, a sensibly improved scenario emerges. The maximum heterogeneity level reached by the current distribution of the PRB180-MEA never reaches value higher than $\varepsilon_{0.25,max}$=20%, while the minimum value is $\varepsilon_{0.25,min}$=14.6% (against the corresponding values of the UNF180-MEA of respectively $\varepsilon_{0.25,max}$=64% and $\varepsilon_{0.25,min}$=44%).

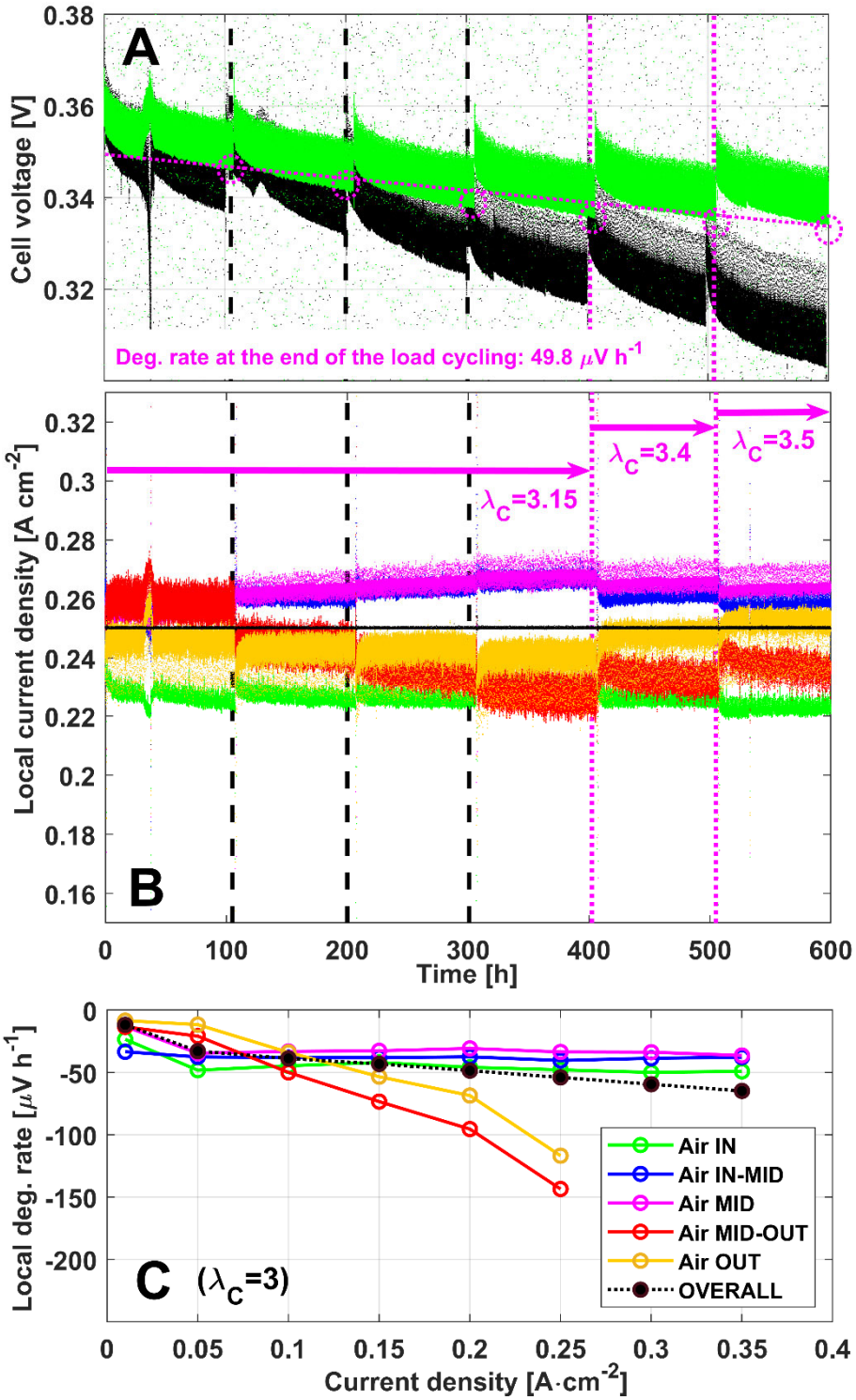

Figure 5 - Evolution during a 600 h degradation test for the PRB180-MEA (purple dotted lines indicate cathode stoichiometry adjustment): A) cell voltage; B) local current density; C) overall and local permanent degradation rate at varying current density, calculated from BoL-EoT iV curves

ECSA trend during the 600 h degradation test (reported as Figure S2B of the supplementary material for the sake of shortness) reveals no significant difference in relative terms with the UNF180-MEA. Again, Figure 5C shows permanent degradation rate calculated from voltage loss between BoL (0 h) and EoT (600 h) local iV curves measured at optimized conditions, confirming strongly more stable operation than that of UNF180-MEA. Indeed, an overall decay rate of 53.8 μV h^{-1} considering the test duration of 600 h (against 148 μV h^{-1} of the UNF180-MEA). It worth to remember that, as discussed in section 2.3.2, for the sake of consistency, iV curves are always measured at nominal operating conditions and hence are directly unaffected by cathode stoichiometry increase strategy adopted during operation. This explains the slightly higher degradation value with respect to that measured from operation (Figure 5A), which is instead positively affected by the increased stoichiometry.

Detailing instead local degradation, a 20-30 mV downward translation of the local iV curves is revealed for inlet to centre regions of the cell (green, blue and purple curves in Figure 5C), related to a 40% ECSA loss from BoL value. Instead, regarding cathode outlet section of the MEA (red and yellow curves in Figure 5C) a different phenomenon appears, with a voltage loss which increases with current density, due to a rotation of the iV curves rather than a pure downward translation.

The increased voltage loss at cathode outlet area is clearly consistent with the localized descending trend of current density during 600 h operation (red, and secondarily yellow in Figure 5B). This effect, present with larger magnitude in UNF180-MEA degradation, is most likely related to mass-transport properties alteration of anode side MPL of the area, as described in [5]. A hydrophobicity loss at anode inlet would determine increased flooding of the facing cathode outlet section, hindering local performance even in presence of a homogeneous ECSA loss [33]. In order to dedicatedly investigate the residual limitations on

performance and fading at cathode outlet sections of the PRB180-MEA, local potential analysis is performed in the next section.

3.3 Local potential analysis

A locally resolved potential analysis has been performed by means of a multiple reference electrodes displacement on the surface of a pristine PRB180-MEA. A set of 6 external RHEs have been connected on the surface of anode and cathode catalyst layers respectively at inlet, centre and outlet sections of both the electrodes, following the methodology discussed in the experimental section.

In the literature, anode overpotential is usually investigated operating the fuel cell in electrolytic mode, feeding the cathode with hydrogen [34], as discussed in section 2. In this configuration DMFC voltage is given by anode and membrane overpotentials. In order to verify the consistency of RHEs measurement, anode potential has been quantified by means of both techniques during DMFC electrolytic operation. Figure 6 depicts the iR-free anodic polarization curve (black solid curve) together with local anode potential measurements (coloured solid curves). The comparison shows a satisfying agreement between the two techniques and, interestingly, a global homogeneity of local potential beneath the three investigated locations in the entire current density range (maximum potential difference of about 35 mV). However, it is worth noting that in DMFC electrolytic operation cathode contribution is negligible, leading to a different interaction with anode electrode compared to the galvanostatic operation.

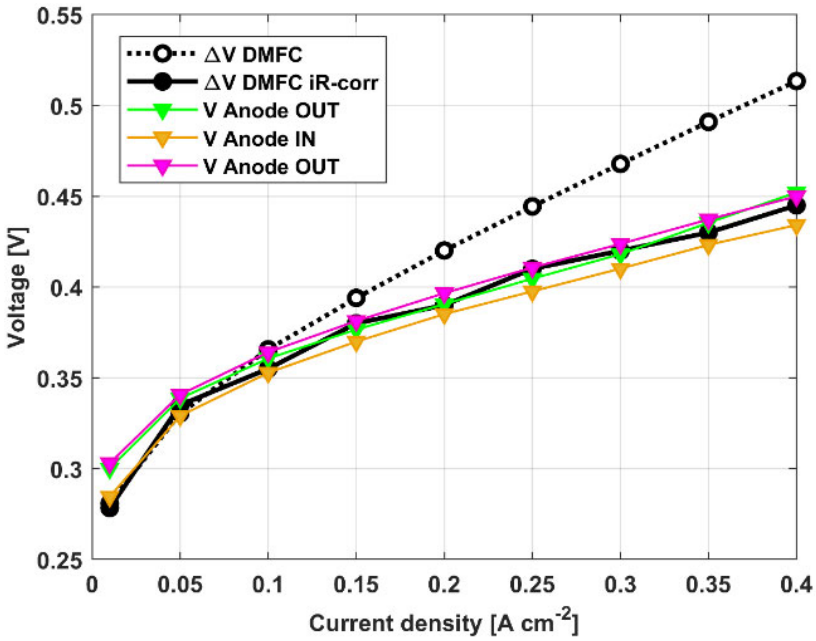

Figure 6 – Comparison of DMFC voltage and iR-corrected value during electrolytic iV curve (black) with local anode potential at inlet, middle and outlet regions (coloured).

Figure 7A compares DMFC polarization curve in reference operating condition along with RHEs potential measurements at both anode and cathode. As expected, inlet and central region of the cell exhibit typical DMFC operating potentials: cathode is about 0.8 V vs RHE, slightly decreasing with increasing current, while anode potential presents a considerable variation, ranging from 0.3 V to 0.5 V [20]. The high value of anode potential at low current is consistent with a previous work by the authors [15], demonstrating that the overpotential associated to methanol oxidation is already 0.2 V at a current density of just 1 mA cm^{-2}. Instead, outlet region potentials exhibit unexpected values: both cathode and anode potential feature very low value (up to 300 mV lower with respect to inlet and central regions). At cathode, such value could be related to a very low oxygen concentration at active sites, while at anode it could indicate a condition in which the local current density is close to zero. However, on this 180PRB-MEA the local current density measured with the m-SFC has a rather homogeneous distribution (see Figure 4), especially at 0.25 A cm^{-2} ($\varepsilon_{0.25}$=11%). Moreover, the inhomogeneous distribution of anode potential is in disagreement with the measurements performed in electrolytic operation

(Figure 6). Clearly, being anode operation mostly unvaried between galvanostatic and electrolytic operation, this redistribution of potential is reasonably attributable to cathode operation, which interacts with anode electrode.

To highlight a possible role of cathode operation, a sensitivity analysis on air stoichiometry is performed. For the sake of shortness, only the results at λ_C=6 are reported and discussed (Figure 6B). Consistently with the expectations, increasing cathode stoichiometry determines an increase of the local potential at cathode outlet and, interestingly, of the corresponding local portion at anode electrode.

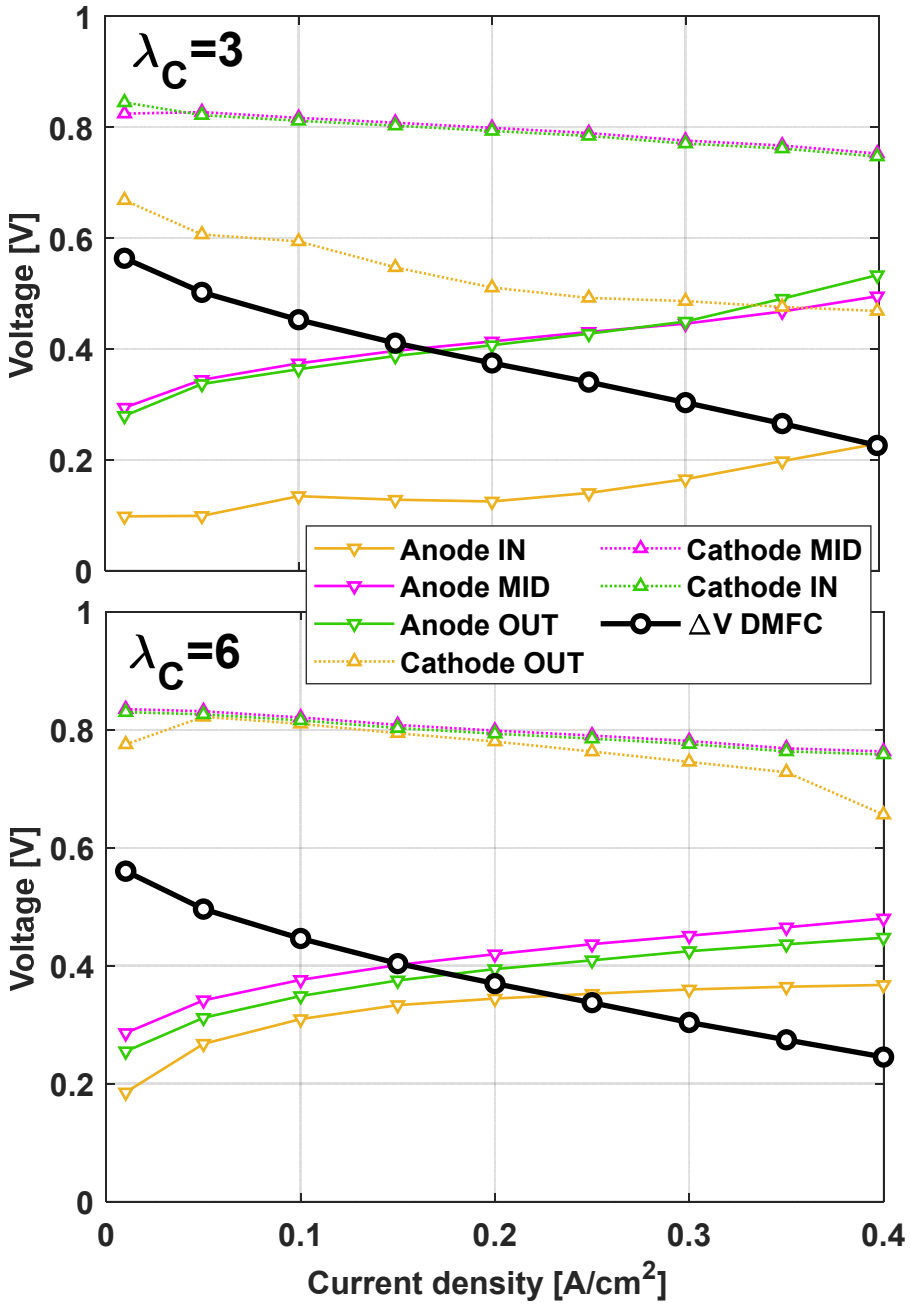

Figure 7 - DMFC galvanostatic iV curve (black) together with local anode and cathode potential (coloured), varying cathode stoichiometry: A) λ_C=3 and B) λ_C=6.

Such strong interaction between anode and a cathode-related parameter can suggest the presence of local hydrogen evolution at anode side at lower air stoichiometry. As described in the introduction section, the HER mechanism has been never identified during nominal operation.

The proposed HEV mechanism leading to low anode local potential during operation is depicted in Figure 8 and described in the following.

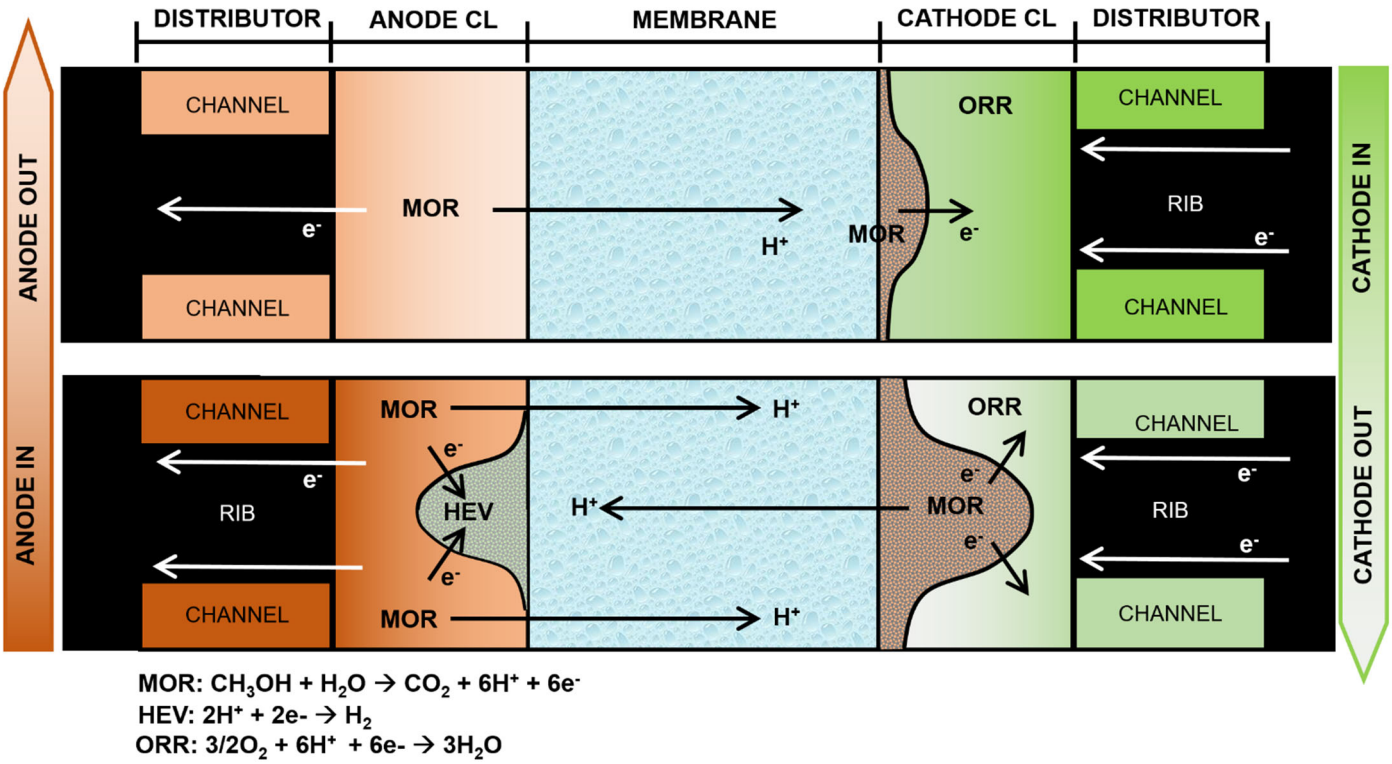

Figure 8 - Scheme of in-operando hydrogen evolution mechanism at cathode outlet region.

At cathode inlet area, where oxygen availability is high, oxygen reduction reaction (ORR) and methanol oxidation reaction (MOR) of crossed-over methanol occur, generating the well-known mixed potential [15]. At cathode outlet, instead, oxygen availability is lower, and the higher water content may lead to electrode flooding, further reducing oxygen concentration. Moreover, due to the higher methanol cross-over form anode inlet, the relative weight of MOR against ORR is increased in this region. In particular, in the area under-the-rib (where the RHE is placed), local oxygen starvation can occur despite the high air stoichiometry (λ_C=3). Here, cathode ORR is inhibited in favour of MOR of crossed-over methanol, leading to a much lower value of cathode potential in consistency with the measurement of Figure 7A. Lack of proton consumption due to reduced oxygen concentration forces excess protons across polymeric membrane, promoting the electrolytic regime of HEV at the corresponding anode region, sensibly decreasing local electrode potential as measured before (Figure 7A). In agreement

with this interpretation and the potential measurements of Figure 7B, an increased air stoichiometry enhances oxygen availability at active sites and thus mitigates HEV, leading to operating potentials more consistent with galvanic operation.

The proposed mechanism is in strong analogy with what already discussed in [13-18], but for the first time it is supposed to take place during nominal operation of a commercial scale DMFC at nominal air stoichiometry. Due to its extremely localized extent, it is important to remark that the macro segmented cell approach was not able to identify the phenomenon.

It is possible to speculate a connection between the localized HEV and the rapid performance fading of outlet area identified during the 600 h degradation test of section 3.2.3, but further studies are necessary to demonstrate the long-term effects of HEV on local performance loss.

4. Conclusions

This work focused on the local investigation of performance and durability of large-scale 180 cm^2 DMFC MEAs coupled with a commercially meaningful distributor geometry. After the characterization of an MEA with uniform cathode CL loading, an optimized MEA has been developed:

- Uniform MEA shows a degradation rate as high as 148 $\mu V\ h^{-1}$ in 600 h test, associated with a strong current redistribution (current dispersion from 32% to 64%). Issues are related to water distribution, leading to dehydration at cathode inlet and flooding at cathode outlet.
- Maintaining the same average loading of the uniform MEA, an optimized MEA has been developed increasing cathode catalyst loading at inlet and outlet regions with a parabolic distribution. The performance distribution at the nominal current is 3 times more homogeneous compared to the uniform MEA (dispersion of 11%) and

permanent degradation rate considerably decreases till 53.8 μV h^{-1} during 600 h degradation test.

Then, the optimized parabolic MEA has been further characterized by means of local RHEs, to investigate residual limitations:

- Anode potential usually measured by means of electrolytic operation is demonstrated to be not representative of local potential distribution of DFMC operation, due to the absence of cathode-anode interplay. This confirms the importance of the developed RHEs setup to characterize local operation.
- Cathode outlet region exhibits anomalies in the measured potential values: for both cathode and anode low potentials are detected, equal to 0.49 V and 0.14 V vs RHE, respectively. This behaviour is addressed to local oxygen starvation under-the-rib, leading to localized HER at the corresponding anode side, whose possible effect on local degradation needs to be further investigated.

Acknowledgements

The research leading to these results has received funding from the European Union's Seventh Framework Program (FP7/2007-2013) for the Fuel Cells and Hydrogen Joint Technology Initiative under grant agreement n°621216 (FCH-JU project Second Act). The authors would like to thank Matteo Agostinelli for the useful help in the experimental activity.

References

[1] X. Li, A. Faghri, Review and advances of direct methanol fuel cells (DMFCs) part I: Design, fabrication, and testing with high concentration methanol solutions, J. Power Sources. 226 (2013) 223–240. https://doi.org/10.1016/j.jpowsour.2012.10.061.

[2] M. Sajgure, B. Kachare, P. Gawhale, S. Waghmare, G. Jagadale, Direct Methanol Fuel Cell: A Review, Int. J. Curr. Eng. Technol. INPRESSCO IJCET Spec. Issue. 6 (2016) 2277–4106.

http://inpressco.com/category/ijcet.

[3] P. Joghee, J.N. Malik, S. Pylypenko, R. O'Hayre, A review on direct methanol fuel cells – In the perspective of energy and sustainability, MRS Energy Sustain. 2 (2015) E3. https://doi.org/10.1557/mre.2015.4.

[4] A. Mehmood, M.A. Scibioh, J. Prabhuram, M.G. An, H.Y. Ha, A review on durability issues and restoration techniques in long-term operations of direct methanol fuel cells, J. Power Sources. 297 (2015) 224–241. https://doi.org/10.1016/j.jpowsour.2015.07.094.

[5] F. Bresciani, C. Rabissi, M. Zago, P. Gazdzicki, M. Schulze, L. Guétaz, S. Escribano, J.L. Bonde, R. Marchesi, A. Casalegno, A combined in-situ and post-mortem investigation on local permanent degradation in a direct methanol fuel cell, J. Power Sources. 306 (2016) 49–61. https://doi.org/10.1016/j.jpowsour.2015.11.105.

[6] P. Karthikeyan, P. Velmurugan, A.J. George, R. Ram Kumar, R.J. Vasanth, Experimental investigation on scaling and stacking up of proton exchange membrane fuel cells, Int. J. Hydrogen Energy. 39 (2014) 11186–11195. https://doi.org/10.1016/j.ijhydene.2014.05.086.

[7] M. Marappan, R. Narayanan, K. Manoharan, M.K. Vijayakrishnan, K. Palaniswamy, S. Karazhanov, S. Sundaram, Scaling Up Studies on PEMFC Using a Modified Serpentine Flow Field Incorporating Porous Sponge Inserts to Observe Water Molecules, Molecules. 26 (2021) 286. https://doi.org/10.3390/molecules26020286.

[8] A. Schröder, K. Wippermann, J. Mergel, W. Lehnert, D. Stolten, T. Sanders, T. Baumhöfer, D.U. Sauer, I. Manke, N. Kardjilov, A. Hilger, J. Schloesser, J. Banhart, C. Hartnig, Combined local current distribution measurements and high resolution neutron radiography of operating Direct Methanol Fuel Cells, Electrochem. Commun. 11 (2009) 1606–1609. https://doi.org/10.1016/j.elecom.2009.06.008.

[9] P. Hartmann, D. Gerteisen, Local degradation analysis of a real long-term operated DMFC

stack MEA, J. Power Sources. 219 (2012) 147–154. https://doi.org/10.1016/j.jpowsour.2012.07.048.

[10] D. Dixon, K. Wippermann, J. Mergel, A. Schoekel, S. Zils, C. Roth, Degradation effects at the methanol inlet, outlet and center region of a stack MEA operated in DMFC, J. Power Sources. 196 (2011) 5538–5545. https://doi.org/10.1016/j.jpowsour.2011.02.007.

[11] T.. Arlt, J.. Author, Manke, I.a, Wippermann, K.b, Riesemeier, H.c, Mergel, J.b, Banhart, Investigation of the local catalyst distribution in an aged direct methanol fuel cell MEA by means of differential synchrotron X-ray absorption edge imaging with high energy resolution, J. Power Sources. 221 (2013) 210–216. https://doi.org/https://doi.org/10.1016/j.jpowsour.2012.08.038.

[12] C. Rabissi, P. Gazdzicki, L. Guétaz, S. Escribano, L. Grahl-Madsen, A. Baricci, A. Casalegno, A locally resolved investigation on direct methanol fuel cell uneven components fading: Steady state and degradation local analysis, J. Power Sources. 397 (2018) 361–373. https://doi.org/10.1016/j.jpowsour.2018.07.034.

[13] C. Rabissi, M. Zago, P. Gazdzicki, L. Guétaz, S. Escribano, L. Grahl-Madsen, A. Casalegno, A locally resolved investigation on direct methanol fuel cell uneven components fading: Local cathode catalyst layer tuning for homogeneous operation and reduced degradation rate, J. Power Sources. (2018). https://doi.org/10.1016/j.jpowsour.2018.09.094.

[14] A. Casalegno, C. Rabissi, L. Grahal-Madsen, Locally engineered PEM cells components with optimized operation for improved durability, PCT patent application n. PCT/IT2007/000120, filed on June 19th, 2017 and published on December 27th, 2018 (Publication No. WO 2018/235108 A1)

[15] M. Zago, A. Bisello, A. Baricci, C. Rabissi, E. Brightman, G. Hinds, A. Casalegno, On the actual cathode mixed potential in direct methanol fuel cells, J. Power Sources. (2016). https://doi.org/10.1016/j.jpowsour.2016.06.093.

[16] A.A. Kulikovsky, H. Schmitz, K. Wippermann, J. Mergel, B. Fricke, T. Sanders, D.U. Sauer, DMFC: Galvanic or electrolytic cell?, Electrochem. Commun. 8 (2006) 754–760. https://doi.org/10.1016/j.elecom.2006.03.011.

[17] H. Dohle, J. Mergel, P.C. Ghosh, DMFC at low air flow operation: Study of parasitic hydrogen generation, Electrochim. Acta. (2007). https://doi.org/10.1016/j.electacta.2007.03.067.

[18] Q. Ye, T.S. Zhao, Electrolytic Hydrogen Evolution in DMFCs Induced by Oxygen Interruptions and Its Effect on Cell Performance, Electrochem. Solid-State Lett. 8 (2005) A211. https://doi.org/10.1149/1.1869012.

[19] Q. Ye, T.S. Zhao, J.G. Liu, Effect of transient hydrogen evolution/oxidation reactions on the OCV of direct methanol fuel cells, Electrochem. Solid-State Lett. (2005). https://doi.org/10.1149/1.2035747.

[20] C. Rabissi, E. Brightman, G. Hinds, A. Casalegno, In operando investigation of anode overpotential dynamics in direct methanol fuel cells, Int. J. Hydrogen Energy. 41 (2016) 18221–18225. https://doi.org/10.1016/j.ijhydene.2016.08.140.

[21] C. Rabissi, E. Brightman, G. Hinds, A. Casalegno, In operando measurement of localised cathode potential to mitigate DMFC temporary degradation, Int. J. Hydrogen Energy. 43 (2018) 9797–9802. https://doi.org/10.1016/j.ijhydene.2018.04.043.

[22] Z. Xia, X. Zhang, H. Sun, S. Wang, G. Sun, Recent advances in multi-scale design and construction of materials for direct methanol fuel cells, Nano Energy. 65 (2019). https://doi.org/10.1016/j.nanoen.2019.104048.

[23] Z. Tan, A. Wang, W. Yuan, F. Han, G. Ye, H. Xia, Y. Tang, Dimensional effect of graphite flow field channels of a direct methanol fuel cell under different operating conditions, Can. J. Chem. Eng. 96 (2018) 659–669. https://doi.org/10.1002/cjce.22995.

[24] T. Kumaresan, T. Velumani, M. Chandran, K. Palaniswamy, A. Thirkell, A. Fly, R. Chen, S.

Sundaram, Effect of Nafion loading and the novel flow field designs on innovative anode electrocatalyst for improved Direct Methanol Fuel cells performance, Mater. Lett. 276 (2020). https://doi.org/10.1016/j.matlet.2020.128222.

[25] S. Sharifi, R. Rahimi, D. Mohebbi-Kalhori, C.O. Colpan, Coupled computational fluid dynamics-response surface methodology to optimize direct methanol fuel cell performance for greener energy generation, Energy. 198 (2020). https://doi.org/10.1016/j.energy.2020.117293.

[26] X. Su, W. Yuan, B. Lu, T. Zheng, Y. Ke, Z. Zhuang, Y. Zhao, Y. Tang, S. Zhang, CO2 bubble behaviors and two-phase flow characteristics in single-serpentine sinusoidal corrugated channels of direct methanol fuel cell, J. Power Sources. 450 (2020). https://doi.org/10.1016/j.jpowsour.2019.227621.

[27] R.M. El-Zoheiry, S. Mori, M. Ahmed, Using multi-path spiral flow fields to enhance under-rib mass transport in direct methanol fuel cells, Int. J. Hydrogen Energy. 44 (2019) 30663–30681. https://doi.org/10.1016/j.ijhydene.2018.11.146.

[28] O. E. Gamea, S. Ookawara, S. Mori, M. Ahmed, Performance enhancement of direct methanol fuel cell using multi-zone narrow flow fields, Int. J. Energy Res. 43 (2019) 8257–8274. https://doi.org/10.1002/er.4822.

[29] and T. Georgios Tsotridis, Alberto Pilenga, Giancarlo De Marco, Malkow, EU Harmonised Test Protocols for PEMFC MEA Testing in Single Cell Configuration for Automotive Applications, JRC Sci. Policy Rep. (2015).

[30] T. Gaumont, G. Maranzana, O. Lottin, J. Dillet, S. Didierjean, J. Pauchet, L. Guétaz, Measurement of protonic resistance of catalyst layers as a tool for degradation monitoring, Int. J. Hydrogen Energy. 42 (2017) 1800–1812. https://doi.org/10.1016/j.ijhydene.2016.10.035.

[31] N. Kimiaie, K. Wedlich, M. Hehemann, R. Lambertz, M. Müller, C. Korte, D. Stolten, Results

of a 20 000 h lifetime test of a 7 kW direct methanol fuel cell (DMFC) hybrid system – degradation of the DMFC stack and the energy storage, Energy Environ. Sci. 7 (2014) 3013–3025. https://doi.org/10.1039/C4EE00749B.

[32] A. Baricci, M. Zago, A. Casalegno, A quasi 2D model of a high temperature polymer fuel cell for the interpretation of impedance spectra, Fuel Cells. 14 (2014) 926–937. https://doi.org/10.1002/fuce.201300147.

[33] F. Bresciani, C. Rabissi, M. Zago, R. Marchesi, A. Casalegno, On the effect of gas diffusion layers hydrophobicity on direct methanol fuel cell performance and degradation, J. Power Sources. 273 (2015) 680–687. https://doi.org/10.1016/j.jpowsour.2014.09.149.

[34] Y.J. Kim, W.H. Hong, S.I. Woo, H.K. Lee, Analysis of the polarization of a direct methanol fuel cell using a pseudo-reversible hydrogen reference electrode, J. Power Sources. (2006). https://doi.org/10.1016/j.jpowsour.2005.11.001.